TISSUE ENGINEERING: Part C
Volume 20, Number 12, 2014

DOI: 10.1089/ten.tec.2013.0701

A Surface-Modified Poly(ε-caprolactone) Scaffold Comprising Variable Nanosized Surface-Roughness Using a Plasma Treatment

HoJun Jeon, MS, Hyeongjin Lee, MS, and GeunHyung Kim, PhD

Melt-plotted poly(ε-caprolactone) (PCL) has been widely applied in various tissue regenerations. However, its hydrophobic nature has hindered its usage in wider tissue engineering applications. In this study, we present the development of a porous and multilayered PCL scaffold, which shows outstanding hydrophilic properties and has a roughened surface consisting of homogeneously distributed nanosized pits. The scaffold was obtained using an innovative oxygen plasma treatment. This technology can induce variable nanoscale surface roughness, which is difficult from traditional plasma treatment. Osteoblast-like cells were cultured on the scaffolds and several cellular responses (cell viability, fluorescence images [live/dead cells, nucleus, and actin cytoskeleton], ALP activity, and calcium mineralization) were assessed for untreated PCL and conventionally plasma-treated PCL scaffolds. The data indicated that an appropriate roughness (654 ± 91 nm) of the PCL scaffold processed with the new plasma treatment induced more advantageous responses for the cells, compared with untreated scaffolds and traditional plasma-treated scaffolds.

Introduction

Solid freeform fabricated poly(ε-caprolactone) (PCL) scaffolds have been widely used as bioactive containers for attachment, migration, and proliferation of seeded cells in various tissue regeneration applications due to the controllable pore structure (pore size and shape, porosity, tortuosity, etc.).[1–4] However, PCL is hydrophobic and has low bioactive properties, resulting in low initial cell attachment and even a reduction in proliferation compared with various natural biopolymers (collagen, alginate, silk fibroin, chitosan, etc.).[5] In addition, the hydrophobic nature of PCL have been a major obstacle to the development of highly porous three-dimensional PCL scaffolds, because these properties prevent seeded cells from infiltrating in the thickness direction and into the middle region of the scaffold. To overcome these problems, some groups have attempted dynamic cell culture using a bioreactor,[6] and various composite systems or coating processes supplemented with various hydrophilic bioactive materials, such as bovine-derived extracellular matrix proteins[6,7] and carbonated hydroxyapatite-gelatin.[8] Several recent reports have outlined successful use of various plasma treatments,[9–11] and 7F2 mouse osteoblasts cultured on PCL-scaffold showed outstanding biological activities, including alkaline phosphatase (ALP) response, osteocalcin protein secretion, and even calcium deposition.[10] Since these plasma treatments have several advantages, such as possibility of changing the surface chemistry and topographical surface property with a great degree of control, without changing the bulk properties of the scaffold and without requiring chemical reagents, the applicability of this technology in tissue regeneration can be expanded.

Along with hydrophilic property of biomaterials, the nano/microtopological surface is a key factor for designing scaffolds. Various studies have shown that the micro-, nano-, and hybrid surface structures resulted in unique biological activities for each topological scale, such as cell adhesion and proliferation. In particular, the nanoscale topological structure (nanogroove pattern, spacing 90 nm, fabricated by electron-beam lithography) has various biological effects on osteoblasts, including their morphology, actin cytoskeleton, and others.[12] In addition, Dalby *et al.*[13] reported that the degree of disorder in the nanoscale pattern (nanopits) on poly(methyl methacrylate) plates had a significant effect on stimulation of bone mineral production by osteoprogenitor cells. Therefore, various techniques have been used to fabricate biomaterials with highly roughened surfaces, such as photolithography,[14] micro-contact printing,[15] colloidal lithography,[16] solvent etching,[17] and plasma processing.[18] Of these techniques, plasma processing has been widely used for surface modification because this process does not require use of toxic solvents, which may affect cellular activities during culture, and does not influence the bulk mechanical properties of the plasma-treated scaffold. Plasma processing has been

Department of Bio-Mechatronic Engineering, College of Biotechnology and Bioengineering, Sungkyunkwan University, Suwon, South Korea.

used not only to confer hydrophilic properties on various hydrophobic biomaterials, but also to fabricate biomaterials with physically roughened nanosurfaces.

Here, we present a new oxygen plasma treatment method, which can modify the PCL scaffolds as hydrophilic and also induce controllable nanoscale surface roughness. To acquire the scaffold, we used PCL scaffolds consisting of multilayered PCL struts. The treated scaffolds were evaluated for not only various physical properties (topographical surface property, tensile property, and dynamic water absorption), but also biological activities by culturing with the MG63 cells. The results of 3-(4,5-dimethylthiazol-2-yl)-2,5-diphenyl tetrazolium bromide (MTT) assay, fluorescence imaging, alkaline phosphatase (ALP), and Ca^{2+} mineralization indicated the plasma-treated PCL scaffold produced using the newly developed exposure technique induced more suitable cellular responses (initial cell adhesion, cell proliferation, and calcium deposition) than those of the PCL scaffolds treated by the conventional plasma-exposure method.

Experimental

Materials and fabrication of melt-plotted PCL scaffolds

PCL (density = 1.135 g/cm^3, molecular weight [M_w] = 90,000, melting temperature = 60°C) was purchased from Sigma-Aldrich (St. Louis, MO). The melt-plotted PCL scaffolds were fabricated using a robot system with three-axis connected to a high-temperature dispenser and a 250-μm dispensing nozzle. PCL powder was shifted to the heating barrel (120°C) of the plotting system, and the temperature of the working stage was set as 28°C. For the first layer, the struts that are perpendicular were dispensed; for the second layer, the struts were plotted with a 100% offset value compared with the previous layer. The third layer was plotted with the same geometry as the first layer. This plotting procedure was repeated twice. In addition, to completely bind between the struts of the layers, we slightly pressed the extruding struts over the previous layer, so that the gap between the nozzle tip and the previous layer was set about 90% compared to the diameter of extruded struts. The speed of the plotter nozzle and applied pneumatic pressure were 3 mm/s and 665 ± 29 kPa, respectively.

Modified oxygen plasma treatment method

Melt-plotted PC scaffolds were processed with oxygen-plasma using LF plasma (CUTE–MP/R; Femto Science, Inc., Gyeonggi, Korea). For the scaffolds, a frequency (50 kHz), power (20 W), pressure (5.3×10^{-1} Torr), spacing gap (40 mm), and oxygen flow rate (10 standard cubic centimeters per minute [sccm]) were used. The plasma chamber was cleaned beforehand by implementing a plasma cycle without samples for 30 min to remove impurities.

PCL scaffolds measuring $10 \times 10 \times 2$ mm^3 were located in the chamber and exposed to the plasma during 1 h for each upside and downside (total exposure time = 2 h). During processing, we used three templates with various hole sizes (100, 500, and 800 nm) (Whatman, Maidstone, Kent, United Kingdom) over the PCL scaffolds. The goal of the templates was to enable selective transmission of ions generated by oxygen plasma. In Figure 1a, a simple schematic using the templates was described.

In this work, an untreated PCL scaffold was used as a control and conventionally plasma-treated PCL scaffolds, which were prepared without any template, were obtained using the following conditions: 20 W, 10 sccm, spacing gap (40 mm), and exposure time of 1 h. In this study, the scaffolds treated with conventional plasma treatment were designated S-CPT and those treated with the templates, 100 and 800 nm, were designated S-PTT-1 and S-PTT-2, respectively.

Characterization of plasma-treated PCL scaffolds

Scanning electron microscopy (SEM, SNE-3000M; SEC, Inc., Gyeonggi-Do, South Korea) was performed to identify the surface morphology of PCL scaffolds.

Atomic force microscopy (AFM) (Nanowizard® AFM; JPK Instruments, Berlin, Germany) was performed for qualitative and quantitative measurement of surface roughness (R_a and RMS) and profile.

The chemical bonding states and atomic concentrations in scaffolds before and after plasma treatment were investigated by X-ray photoelectron spectroscopy (XPS) (ESCA2000; VG Microtech, Uckfield, United Kingdom) using a hemispherical electrostatic energy analyzer and an Al K_α (1486.6 eV) X-ray source. The base-pressure in the sample chamber was regulated to 10^{-9} Torr. The measured spectra were displayed as plots of the amount of electrons versus the electron binding energy at a fixed, small-energy interval. For quantification peak area and peak height sensitivity factors were used. All surface compositions mentioned here are indicated as atm%. The four measurements were carried out to obtain each date point and averaged the values. By using a nonlinear least squares algorithm with a Shirley base line and a Gaussian–Lorentzian combination, XPS spectra were deconvoluted. XPS Peak-Fit 4.1 software was run for all data processing.

To measure the wetting properties of the samples, one droplet (10 μL) of the mixture of water and red dye was carefully dropped onto the surface of the scaffolds, and the wetting behavior was captured with a digital camera for various periods.

Absorption of water was calculated by measuring the weight of the samples before and after soaking in distilled water for 2 h. Percentage increase in water absorption was considered as $(\%) = (W_{2h} - W_0)/W_0 \times 100$, where W_{2h} was the weight of samples after 2 h and W_0 was the original weight of the sample at time zero.

To measure the tensile properties, the scaffolds were divided into small strips (8×20 mm^2). The tests were conducted using a tensile machine (Top-tech 2000; Chemilab, Kyunggi-Do, South Korea). The stress and strain results for the scaffolds were measured at a stretching speed of 0.5 mm/s. Measured values are given as the mean ± standard deviation ($n = 5$).

In vitro *cell culture*

PCL scaffolds ($5 \times 5 \times 2$ mm^3) were sterilized with 70% ethanol and ultraviolet (UV) light, and then put in culture medium overnight (24-well plate and 1 mL of medium). MG63 (MG63-human source, ATCC number CRL-1427; ATCC, Manassas, VA) were applied to evaluate the cellular responses cultured on the scaffolds. The cells were cultured for up to five passages in 24-well plates containing Dulbecco's modified Eagle's medium (DMEM; Hyclone, Thermo Scientific, Logan, UT) supplemented with 10% fetal bovine serum (FBS; Hyclone) and 1% penicillin–streptomycin (Hyclone).

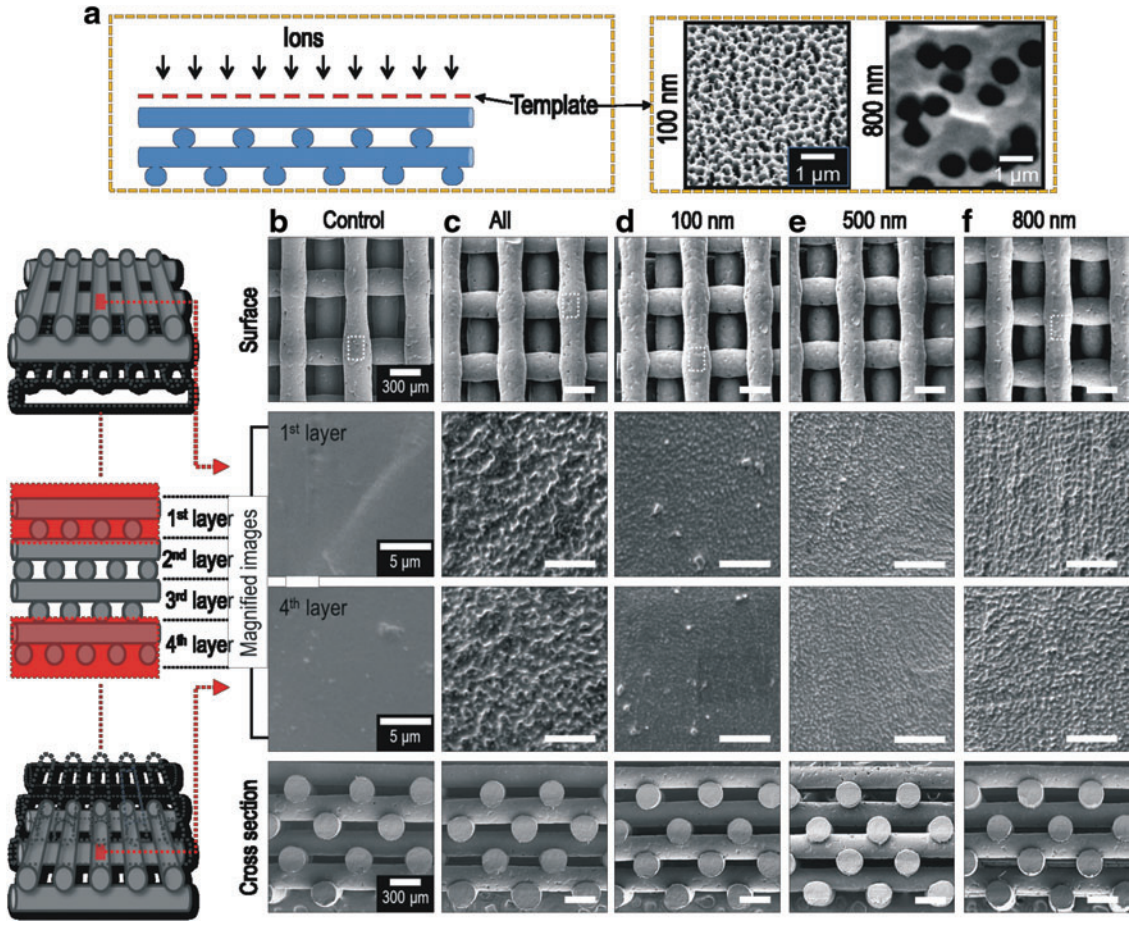

FIG. 1. **(a)** Schematic of the plasma treatment on the scaffold and scanning electron microscopy images of two different templates (100 and 800 nm). Surface and cross-sectional scanning electron micrographs of **(b)** control, **(c)** PCL scaffold with the conventional plasma treatment (S-CPT), and PCL scaffolds treated with templates with hole sizes: **(d)** 100 nm (S-PTT-1), **(e)** 500 nm, and **(f)** 800 nm (S-PTT-2). PCL, poly(ε-caprolactone). Color images available online at www.liebertpub.com/tec

The cells were gathered by trypsin–ethylenediaminetetraacetic acid (EDTA) treatment. Cells (1×10^5 cells) were diluted into 30 μL of medium and added to the top of the scaffold in 24-well plate, and allow to preferentially adhere to scaffold before addition of the full volume (500 μL) of medium during 4 h in CO_2 incubator (37°C and 5% CO_2). The medium was altered every second day.

After 4 h and 1 day in cell culture, the scaffolds were exposed to 0.15 mM calcein AM and 2 mM ethidium homodimer-1 for 45 min in an incubator to permit observation of live and dead cells. The stained specimens were visualized under a microscope (TE2000-S; Nikon, Tokyo, Japan) prepared with an epifluorescence attachment and a SPOT RT digital camera (SPOT Imaging Solutions, Sterling Heights, MI). Stained images were captured, in which green and red indicated live and dead cells, each. The Image J software (National Institutes of Health, Bethesda, MD) was accommodated to enumerate live cells in the width direction of the scaffolds after 1 day of culture.

After 4 h and 1 day of cell culture, the scaffold was gently washed with phophate buffered saline (PBS) and fixed in 4% paraformaldehyde for 30 min, permeabilized with 0.1% Triton X-100 for 5 min. The scaffolds were susceptible to diamidino-2-phenylindole (DAPI) fluorescence staining to spot cell nuclei. Phalloidin (Invitrogen, Carlsbad, CA) staining was done to make the actin cytoskeleton of proliferated cells visible. A laser-scanning microscope (LSM510; Carl Zeiss, Oberkochen, Germany) was used to achieve the images.

Cell viability was determined by MTT measurement (Cell Proliferation Kit I; Boehringer Mannheim, Mannheim, Germany). The MTT-assay was established on cleavage of the yellow tetrazolium salt MTT by mitochondrial dehydrogenases in viable cells to generate purple formazan crystals. Cell/scaffolds were put in incubation with 0.5 mg mL^{-1} MTT for 4 h at 37°C. The absorbance at 570 nm was measured using a microplate reader (EL800; Bio-Tek Instruments, Winooski, VT). Five samples were used for each incubation period, and each test was measured in triplicate.

ALP activity and alizarin red S staining

ALP was measured with the release of *p*-nitrophenol (pNP) from *p*-nitrophenyl phosphate (pNPP). PCL scaffolds seeded with MG63s were mildly rinsed with PBS and incubated in Tris buffer (10 mM, pH 7.5) containing 0.1% Triton X-100 surfactant for 10 min. Then, 100 μL of the lysate were added to the wells of 96-well tissue culture plates composed of 100 μL of pNPP solution, put together

using an ALP kit (procedure no. ALP-10; Sigma-Aldrich). In the presence of ALP, pNPP is converted to pNP and inorganic phosphate. The activity of ALP was decided from the absorbance at 405 nm by means of a microplate reader (Spectra III; SLT Lab Instruments, Salzburg, Austria). The optical density (OD) of ALP activity was divided with the total protein content (OD value).

Calcium deposition was decided by alizarin red S staining of MG63 cells in 24-well plates. MG63 cells were cultivated in DMEM composed of 50 μg/mL vitamin C and 10 mM β-glycerophosphate. Then, the cells were cleansed thrice with PBS, fixed in 70% (v/v) cold ethanol (4°C) for 1 h, and air-dried. The ethanol-fixed specimens were stained with 40 mM alizarin red S (pH 4.2) for 1 h and cleansed thrice with purified water. Afterward, specimens were destained with 10% cetylpyridinium chloride in 10 mM sodium phosphate buffer (pH 7.0) for 15 min. An optical microscope was accommodated to observe the staining region, and the OD was measured at 562 nm by means of a Spectra III UV microplate reader. The OD was divided to the total protein content (OD value).

Total protein content and protein absorption

The total amount of protein content was estimated by bicinchoninic acid (BCA) protein assay (Pierce Kit; Thermo Scientific). The samples were assayed after cell culture 7 and 14 days. Specimens were cleansed with PBS and lysed with 1 mL of 0.1% Triton X-100. An aliquot of the lysate (25 μL) was added to 200 μL of BCA working reagent. The mixture was left in incubation for 30 min at 37°C. Using a plate reader, the absorbance at 562 nm was determined.

To measure the protein absorption, the scaffolds without cells were put in 96-well plate composed of DMEM with 10% FBS and left in incubation at 37°C for the time periods (1, 2, 4, 6, and 12 h). Next procedure was completely same with the method measuring the total protein content. As a blank, the scaffolds with serum-free medium were used. The protein absorption was given as mean ± standard deviation ($n = 5$).

Statistical analyses

Measured data are given as mean ± standard deviation. Statistical analyses were done by means of SPSS software (ver. 20.0; SPSS, Inc., Chicago, IL), and those included single-factor analyses of variance. In this study, $*p < 0.05$ was regarded to show statistical significance. ''NS'' shows no significant difference.

Results and Discussion

Morphology of fabricated scaffolds

Figure 1b–f indicates the SEM images of control and finally fabricated PCL scaffolds (plasma-treated PCL scaffolds with and without templates). In the images, ''all'' indicates the PCL scaffold treated with a conventional plasma-treatment method and ''100, 500, and 800 nm'' indicate the PCL scaffolds treated with the templates (hole size: 100, 500, and 800 nm, respectively). As indicated in the cross-sectional images, each layer of PCL struts was well offset from the previous layer (100% offset). As reported by several groups, the offset scaffolds showed increased bioactive properties (higher cell seeding efficiency, cell viability, and ALP activity) due to the active contact reaction between cells and osteogenic fluid.[19,20]

Generally, pore size of scaffolds has been an important design factor since it directly affects the mechanical properties, porosity, and various cellular responses (cell proliferation and mineralization). According to O'Brien and colleagues, proper pore size of 300–400 μm was suggested for hard tissue regeneration.[21] Therefore, we designed the scaffolds with a 400 μm pore size. Table 1 shows the detailed geometries of the scaffolds, including strut size ($p > 0.05$), pore size ($p > 0.05$), and porosity ($p > 0.05$). In Table 1, although the pore size did not completely match with the designed pore size, all scaffolds exhibited a reasonable pore size range (460–470 μm). In addition, the strut size (290–296 μm) and porosity (47–49%) of the scaffolds were similar.

Figure 1b–f show magnified surface images of the PCL scaffolds. As indicated in the SEM images, the PCL strut-surfaces treated with plasma were highly roughened. Interestingly, the PCL struts treated with templates (hole size = 100, 500, and 800 nm) exhibited homogeneously sized and randomly distributed nano-pit structures compared with untreated surfaces and those that underwent conventional plasma treatment. Also, on the basis of the magnified images, the sizes of the nano-pit on the scaffolds can be controlled by the template size used in the plasma process. Furthermore, the patterned surface of 1st and 4th layer of the treated scaffolds was similar.

Surface roughness

The nanosized patterns provided several biological cues, which induced not only increased actin cytoskeleton organization and integrin-meditated adhesion, but also selective modulation of osteogenic differentiation.[13,22–24] Therefore, the relationships between various surface physical patterns and several cell types (fibroblast, macrophage, endothelial, and osteoblast) have been investigated.[22] In particular, the activities (cell morphology, actin cytoskeleton, adhesion, differentiation, etc.) of osteoblasts in various nanosized surface structures, nanogrooves, and nanosized islands were investigated.[12,22,23]

To observe the fabricated surface pattern on the PCL scaffolds, we measured the surface roughness of plasma-treated PCL struts using AFM. Roughened surfaces of

Table 1. Measured Pore Structure (Strut Size, Pore Size, and Porosity) of Scaffolds

	Control	*S-CPT*	*S-PTT-1*	*S-PTT-2*
Strut size (μm)	295.9 ± 17.7	295.7 ± 17.9	289.8 ± 19.4	293.7 ± 17.6
Pore size (μm)	461.8 ± 10.9	459.8 ± 11.2	454.9 ± 12.47	465.8 ± 19.61
Porosity (%)	47.7 ± 1.3	48.07 ± 1.9	48.7 ± 1.3	48.72 ± 1.6

scaffolds produced using the control, conventional plasma treatment (S-CPT), and new plasma-treatment processes using the 100 (S-PTT-1) and 800 nm (S-PTT-2) templates are shown in Figure 2a. The PCL scaffolds treated with plasma/templates showed nanosized pits, whereas S-CPT exhibited microsized pit structures. The surface topological profiles were plotted in Figure 2b. The roughness (R_a) data presented in Figure 2c were obtained using the equation: $R_a = (\int |f(x)|dx)/L$, where L is the length and $f(x)$ stands for the roughness curve in Figure 2b.

The surface profile indicated that the untreated PCL struts (control) showed relatively smooth surfaces with roughness of 23 ± 6 nm, and S-CPT has a highly roughened surface of 1.9 ± 0.2 µm, while S-PTT-1 and S-PTT-2 had roughness values of 93 ± 10 and 654 ± 71 nm, respectively. Interestingly, the roughness of the pattern increased with increasing template hole size.

Chemical characterization of the plasma-treated PCL scaffold surface

Figure 3a–d show XPS spectra of control, S-CPT, and S-PTT-1, and S-PTT-2 scaffolds, respectively. The peak analysis results are summarized in Table 2 (chemical composition [%] and relative area corresponding to various types of chemical bond [%]).

The oxygen content (O/C) ratio of PCL surfaces exposed to oxygen plasma is increased.[25] As shown in the table, the surface characteristics of the control showed oxygen and carbon levels of 20.75% and 79.25%, respectively, which were altered to 23.45% and 76.55% in the plasma-treated PCL scaffold without a template. However, oxygen levels were significantly increased by ~31% and 29% for treated PCL scaffolds produced by means of the templates (100 and 800 nm) compared with the control, respectively.

Interestingly, meaningful difference between S-CPT and S-PTT scaffolds was observed in the intensity of the peaks due to the selective plasma-exposure area and time. The XPS data showed the O/C increases due to the surface oxidation of the scaffolds treated with plasma, and the increase of the oxygen was dependent on the treatment methods for S-CPT and S-PTT. According to Habibovic and colleagues, the increase of the oxygen component can induce to present high hydrophilic property of scaffold in which the increase can be attributed to the presence of oxygen groups.[25] From the XPS results, we can confirm that the selective plasma treatments lead to different surface chemistry, which can affect the hydrophilicity and the initial cell adhesion.

Wettability, water absorption, and protein absorption

To examine the hydrophilic properties of the PCL scaffold, we measured dynamic water wettability and water absorption. The water absorption and wettability of biomedical scaffolds have significant effects on cell migration and proliferation, and morphology.[26]

Figure 4a–d show the dynamic wettability at various time points (1, 10, 30, and 60 s). The control showed a high water contact angle ($113° \pm 1.5°$ at the initial stage, $100° \pm 2°$ at 60 s). However, for the plasma-treated PCL scaffolds (S-CPT, S-PTT-1, S-PTT-2), the water droplet was completely absorbed within the scaffold, indicating fully hydrophilic properties.

These results indicated that the plasma-treated PCL scaffolds were hydrophilic, facilitating homogeneous infiltration of seeded cells.

Figure 4e shows the water absorption by the scaffolds. The plasma-treated PCL scaffolds showed 2.5-fold greater water absorption than the control. As indicated by previous wettability results, the water absorption of the plasma-treated scaffolds did not differ significantly, indicating that the hydrophilicity of the plasma-treated scaffolds was not dependent on template usage during plasma exposure. Such good wettability and improved water absorption of the

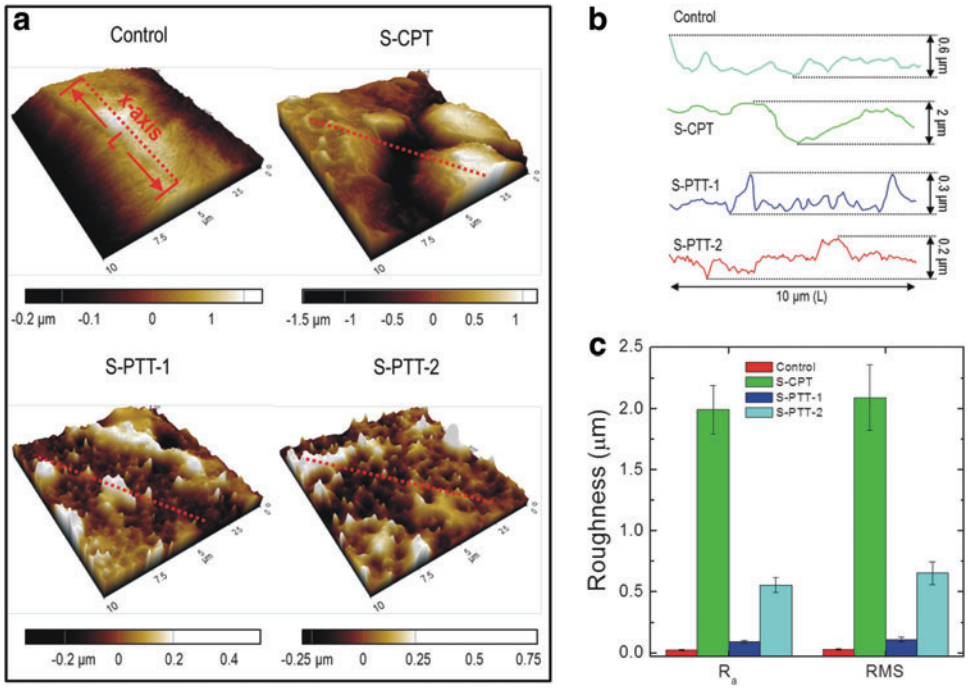

FIG. 2. **(a)** Three-dimensional topographical images (atomic force microscopy [AFM] images) of control, S-CPT, S-PTT-1, and S-PTT-2 scaffolds, **(b)** single lines of the roughened surfaces of the AFM images, and **(c)** average roughness (R_a and RMS) values of the surfaces. AFM, atomic force microscopy. Color images available online at www.liebertpub.com/tec

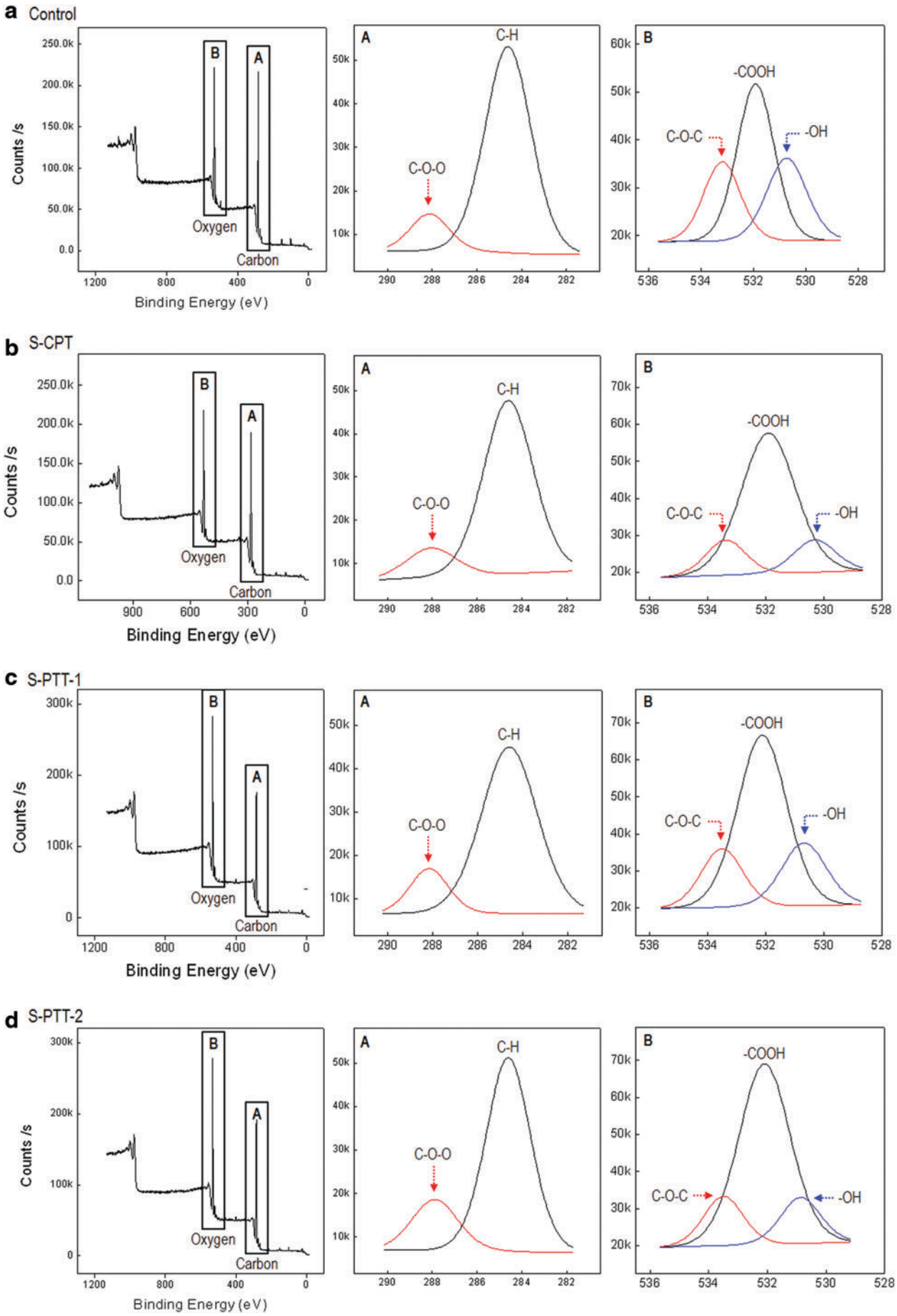

FIG. 3. X-ray photoelectron spectroscopy results for **(a)** the control, **(b)** S-CPT, **(c)** S-PTT-1, and **(d)** S-PTT-2 scaffolds. Color images available online at www.liebertpub.com/tec

TABLE 2. X-RAY PHOTOELECTRON SPECTROSCOPY DATA FOR CONTROL AND PLASMA-TREATED POLY(ε-CAPROLACTONE) SCAFFOLDS

	Chemical composition (%)		*Relative area corresponding to different chemical bonds (%)*				
			Carbon		*Oxygen*		
Condition	*Carbon*	*Oxygen*	*C-H*	*C-O-O*	*-COOH*	*C-O-C*	*-OH*
Control	77.07	22.93	66.99	10.08	11.09	5.57	6.27
S-CPT	75.53	24.47	64.6	10.93	17.96	3.31	3.2
S-PTT-1	71.29	28.1	60.12	11.17	17.29	5.02	5.79
S-PTT-2	72.34	27.06	56.86	15.48	19.2	4.04	3.82

plasma-treated PCL scaffolds would help to avoid the loss of body fluid and various nutrients for *in vitro* and *in vivo* applications.

Protein absorption of the scaffold is an important factor to affect cellular responses (cell proliferation and differentiation).[27] The protein absorption was performed with the control and plasma-treated scaffolds for various periods of 1, 2, 4, 6, and 12 h, respectively. In Figure 4f, as enhancing the incubating period, the protein adsorption for all scaffolds was gradually increased. Interestingly, the plasma-treated scaffolds (S-CPT, S-PTT-1, and S-PTT-2) showed significant increase of protein deposition, compared to that of the control scaffold due to the roughened surface, which can be used in protein-binding sites. However, we cannot find the difference of the protein absorption at 12 h between the S-CPT and S-PTT scaffolds ($p > 0.05$)

Tensile properties

One of the major advantages of plasma treatment is the minimal damage to the bulk mechanical properties of plasma-treated materials. To assess the differences in their tensile properties for the scaffolds, we performed the testing for the control and plasma-treated PCL scaffolds. Figure 5a shows the stress and strain curves for the scaffolds. The mechanical analysis was performed using the tensile mode with a stretching speed (0.5 mm s^{-1}). In general, pore-structured follow a curve common to porous materials,

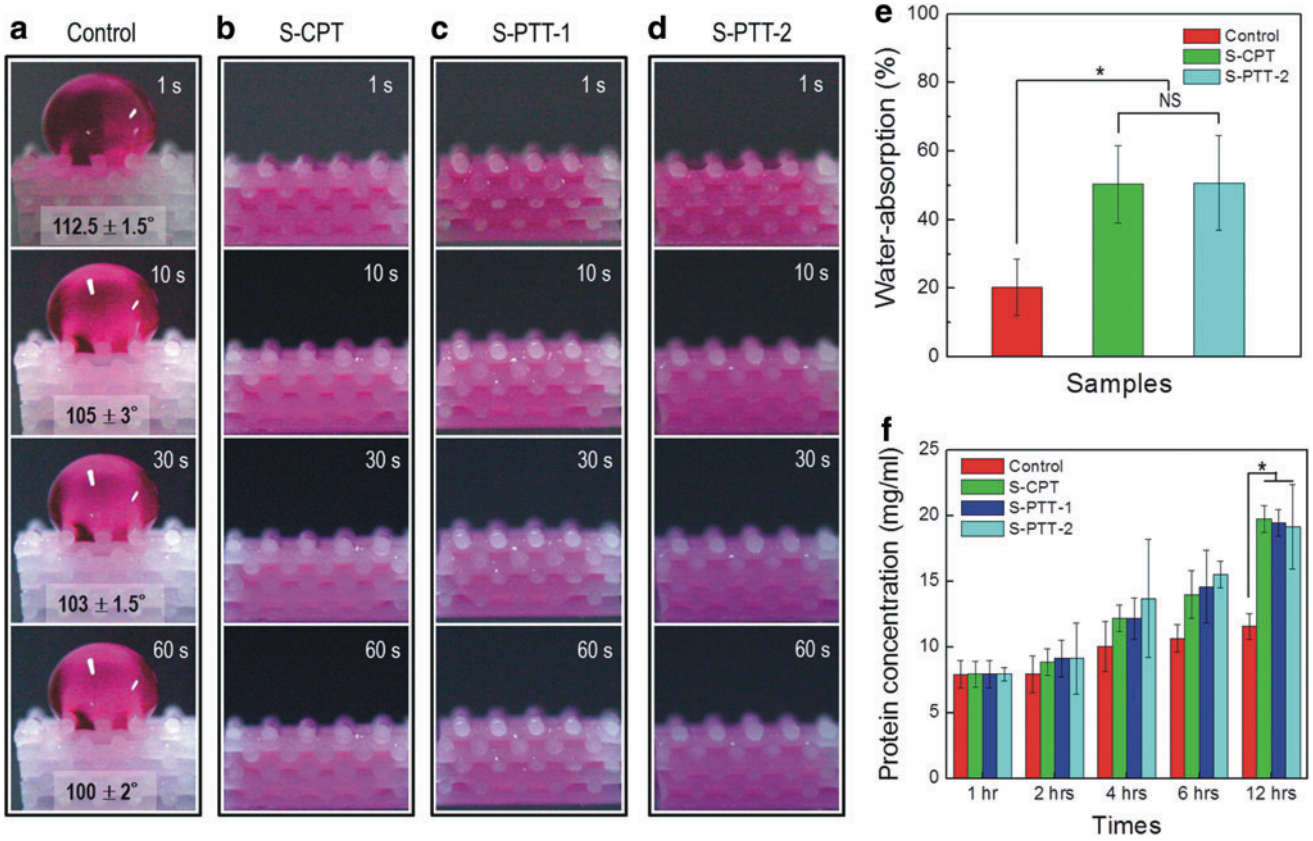

FIG. 4. **(a–d)** Dynamic wettability of one droplet (10 μL) of water mixed with red dye (the contact angles between 1 s and 10s, $p < 0.05$) and **(e)** water absorption (%) after 2 h by the various PCL scaffolds ($n = 5$). **(f)** Protein absorption results for the scaffolds. *$p < 0.05$. NS, no significant difference. Color images available online at www.liebertpub.com/tec

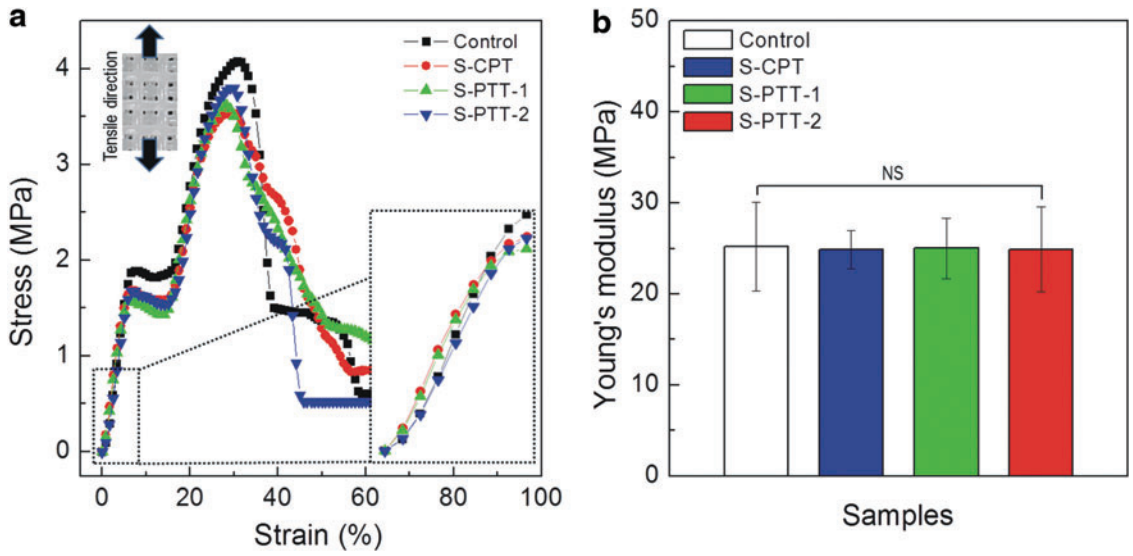

FIG. 5. **(a)** Stress–strain curves for the scaffolds. **(b)** Comparison of Young's moduli for the PCL scaffolds ($n = 5$). Color images available online at www.liebertpub.com/tec

showing a linear curve in an elastic zone at initial stretching stage, a plateau region, and an extensional hardening zone.[28] Figure 5b shows the Young's moduli of the scaffolds. The moduli of the control and plasma-treated PCL scaffolds were similar, ranging from 24.9 to 25.2 MPa for a given stretching speed. Statistical analysis showed no significant differences ($p > 0.05$) for the moduli of the control and plasma-treated scaffolds. These results indicated that plasma treatment had no effect on the Young's modulus of the PCL scaffolds, although the maximum tensile strength and break strain showed slightly different values between the control and plasma-treated scaffolds.

In vitro *culture using MG63 cells*

Initial cell attachment and viability are important parameters to obtain successful tissue growth using various scaffolds, as they markedly influence various cellular responses, including proliferation and distribution within the scaffold as well as tissue regeneration time.[29] To assess initial cell attachment and viability, live/dead staining was performed at 4 h and 1 day after cell seeding using calcein AM and ethidium homodimer 1, respectively.

Figure 6a shows fluorescence images of the scaffolds (control, S-CPT, S-PTT-1, S-PTT-2, respectively) at 4 h, in which live and dead cells are green and red, respectively. As shown in the result, the initial live cells displayed good attachment to the plasma-treated scaffolds compared with the control. Interestingly, for the plasma-treated scaffolds S-PTT-1 and S-PTT-2, the initially attached cells showed significantly higher viability and a well-stretched shape compared with the control.

To observe the initial cell distribution throughout the scaffolds, we visualized live cells in the cross-sectional area after 1 day of cell culture, as homogeneous cell distribution in the interior structure can lead to efficient functionality of the regenerated tissues.[30] Figure 6b shows the live cell distribution in a cross-sectional view of the scaffolds. Live cells were enumerated in each layer (layers 1, 2, 3, and 4 of the scaffold) (Fig. 6c). Cells with an ECM in the plasma-treated PCL scaffolds (S-CRT, S-PTT-1, and S-PTT-2) were distributed more homogeneously than cells in the control scaffolds (Fig. 6d). In Figure 6d, the cell distribution was calculated based on the number of cells in each layer in Figure 6c.

Figure 7a–d show staining of nuclei and F-actin in the scaffolds (blue and red, respectively). At 4 h, significant differences in cell morphology between control and plasma-treated scaffolds (S-PTT-1 and S-PTT-2) were observed. In the control and S-CPT scaffolds, the cells formed islands and the actin cytoskeleton was not fully stretched (Fig. 7a, b), indicating low affinity with the scaffold. However, the cells on the scaffold-surfaces (S-PTT-1 and S-PTT-2) treated with the templates exhibited a well-spread, assembled, and multilateral-shaped structure with well-developed actin fibers in the cytoskeleton (Fig. 7c, d). In addition, greater numbers of cells were observed on the S-PTT scaffold compared with the control and S-CPT scaffolds, indicating a high level of cell-to-cell interactions.

At 1 day, although the actin filaments were well developed in the control and S-CPT scaffolds, the actin filaments in the S-PTT-1 and S-PTT-2 scaffolds were also more highly developed and stretched on the nano-pit surfaces.

Figure 8a shows the cell viability of the various PCL scaffolds, as determined by MTT. In the results, we set the control scaffold as 100%, so that the viabilities of S-CPT and S-PTT scaffolds were relative value for the control scaffold. The numbers of viable cells attached to the treated PCL scaffolds were considerably higher than in the control ($p < 0.05$). Furthermore, the PCL scaffolds (S-PTT-1 and S-PTT-2) treated with the 100- and 800-nm templates showed markedly higher numbers of viable cells at 7 days compared with the S-CPT scaffold (treated with the conventional plasma exposure method), indicating that the plasma-etched nanosized pits on the surface of the scaffolds played a prominent role in various cellular activities (cell attachment and proliferation). This was likely because the cellular responses of viable cells was extremely associated with not

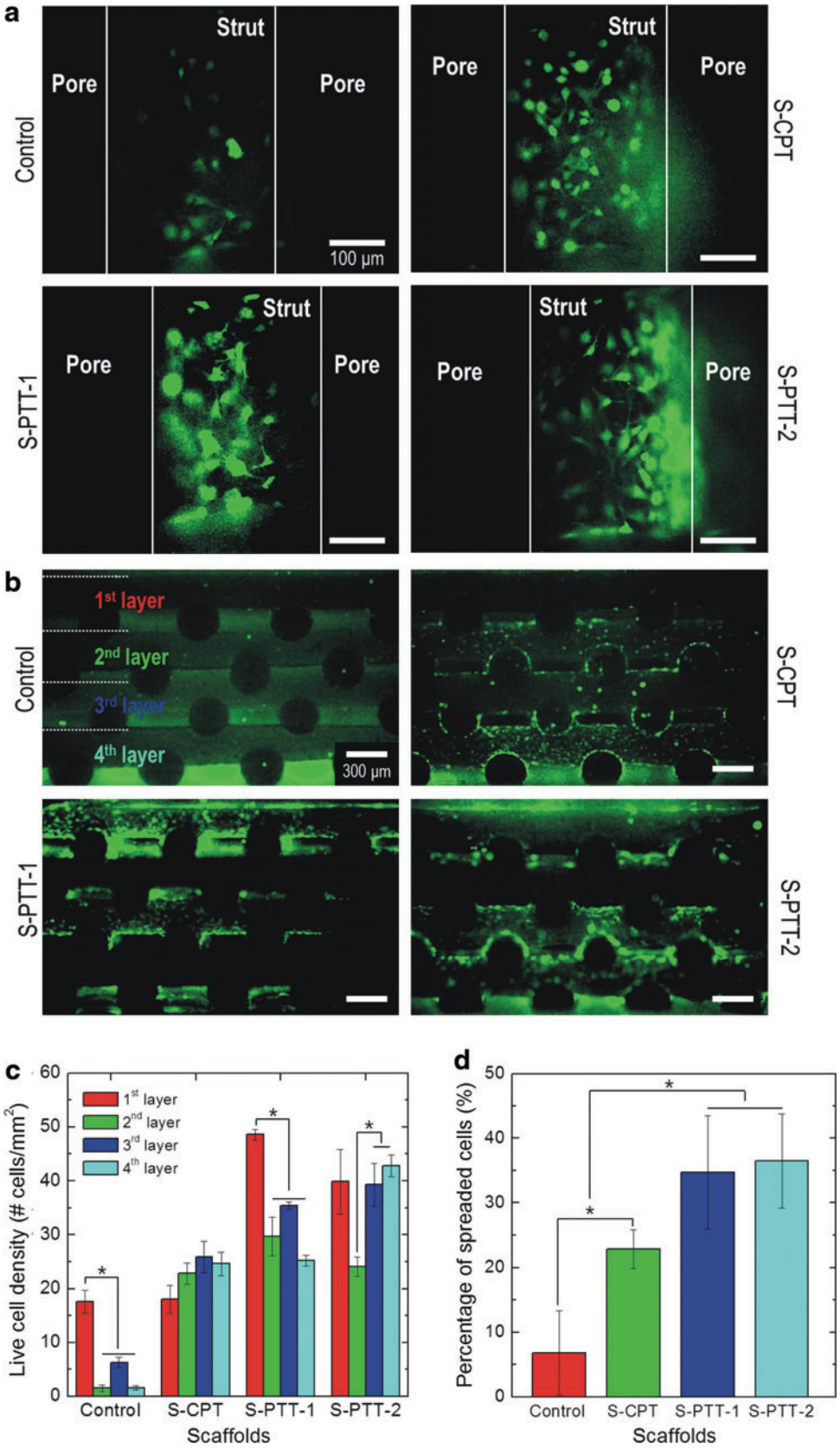

FIG. 6. Live (green) and dead (red) MG63 cells after **(a)** 4 h and **(b)** 1 day of culture on various scaffolds. The images of scaffolds cultured for 1 day are cross-sectional views showing the cell distribution in each layer. **(c)** Cells in each layer of the scaffolds were enumerated using Image-J, and **(d)** the distribution of cells calculated from the number of cells in each layer. $*p < 0.05$. Color images available online at www.liebertpub.com/tec

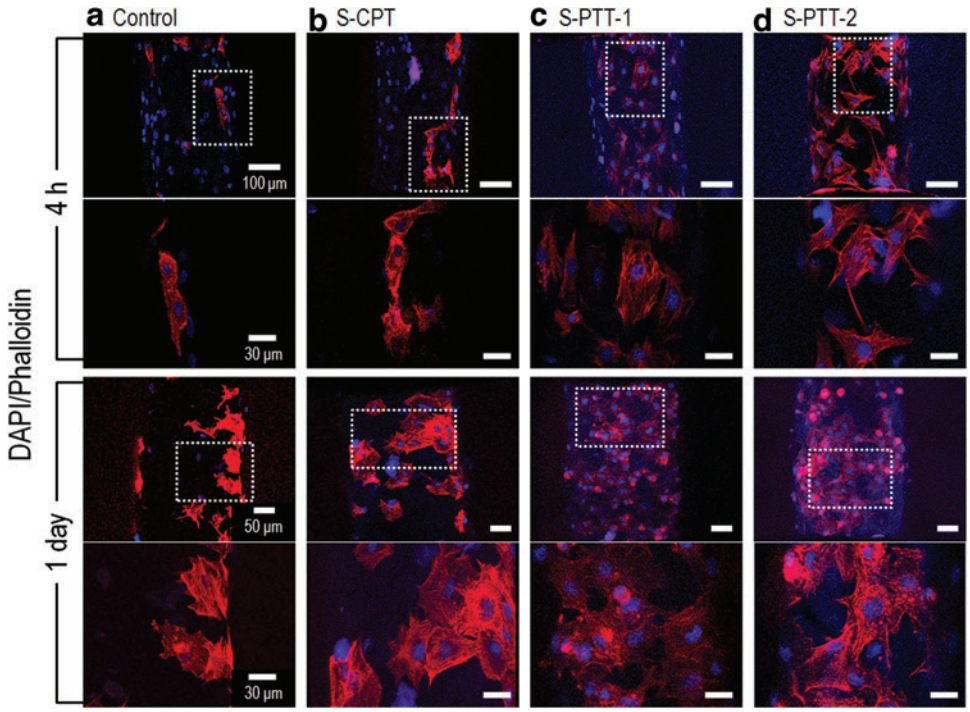

FIG. 7. DAPI/phalloidin images after cell culture for 4 h and 1 day for **(a)** control, **(b)** S-CPT, **(c)** S-PTT-1, and **(d)** S-PTT-2 scaffolds. DAPI, diamidino-2-phenylindole. Dotted square boxes were magnified. Color images available online at www.liebertpub.com/tec

only the physical properties (i.e., hydrophilicity and rapid wettability), but also with the nano-roughened surface.

Figure 8b shows the increasing rate (slope) of viable cells versus the culture days (3 and 7 days) for the control and plasma-treated scaffolds. As shown in the result, the increasing rate of the viable cells for control, S-CPT, and S-PTT-1 scaffold were nonsignificant, but the value of the S-PTT-2 scaffold was evidently high, indicating that the nano-roughened surface of S-PTT-2 scaffold can provide the most effective microenvironmental condition to the cells, compared with other scaffolds.

ALP activity and calcium mineralization

ALP activity has been used as an early osteoblastic differentiation marker. It is highly related with the cells showing the mineralization of extracellular matrix (ECM). In Figure 9a, the ALP activity, which was normalized to the total protein content, of the MG63s on the control and treated PCL scaffolds was determined at 7 and 14 days. The total protein content was described in Table 3. We set the value of the control as 100%, and those for the other scaffolds are shown as relative values. The relative ALP activity was increased in all scaffolds with increasing culture duration. At 7 days, with the exception of S-PTT-2, all scaffolds showed similar activities, while at 14 days the ALP activities of plasma-treated scaffolds (S-PTT-1 and S-PTT-2) were meaningfully higher than those of the control and S-CPT scaffolds. This was due to induction of signaling by the nanoscale surface patterns of the plasma-treated PCL scaffolds (S-PTT-1 and S-PTT-2), to regulate the fate of cells on the surface.[25] Interestingly, S-PTT-2 showed the highest ALP activity. We cannot explain this observation. However, in previous studies, MG63 cultured for 14 days were imprinted on PDMS surfaces.[31] The MG63 cells on the imprinted surface ($R_a = 702 \pm 87$ nm) were re-cultured and

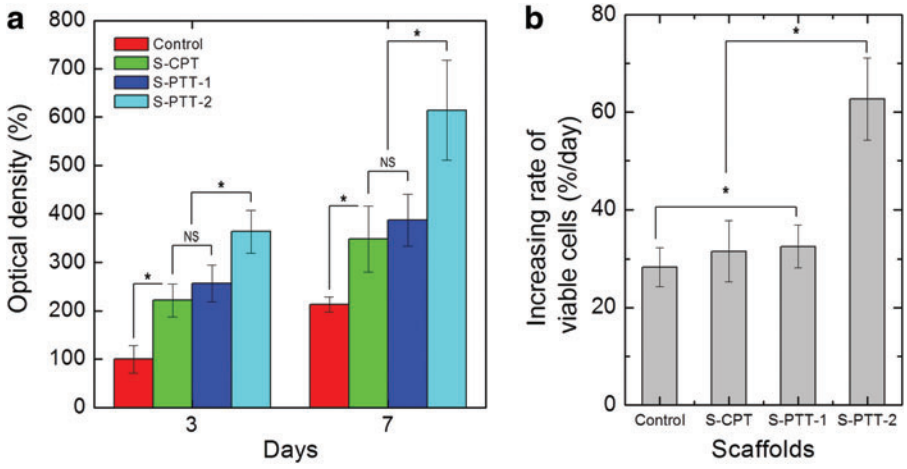

FIG. 8. **(a)** MG63 cell viability at 3 and 7 days on control, S-CPT, S-PTT-1, and S-PTT-2 scaffolds as indicated by MTT assay. **(b)** Increasing rate of viable cells in the scaffolds for the time periods. MTT, 3-(4,5-dimethylthiazol-2-yl)-2,5-diphenyl tetrazolium bromide. *$p < 0.05$. Color images available online at www.liebertpub.com/tec

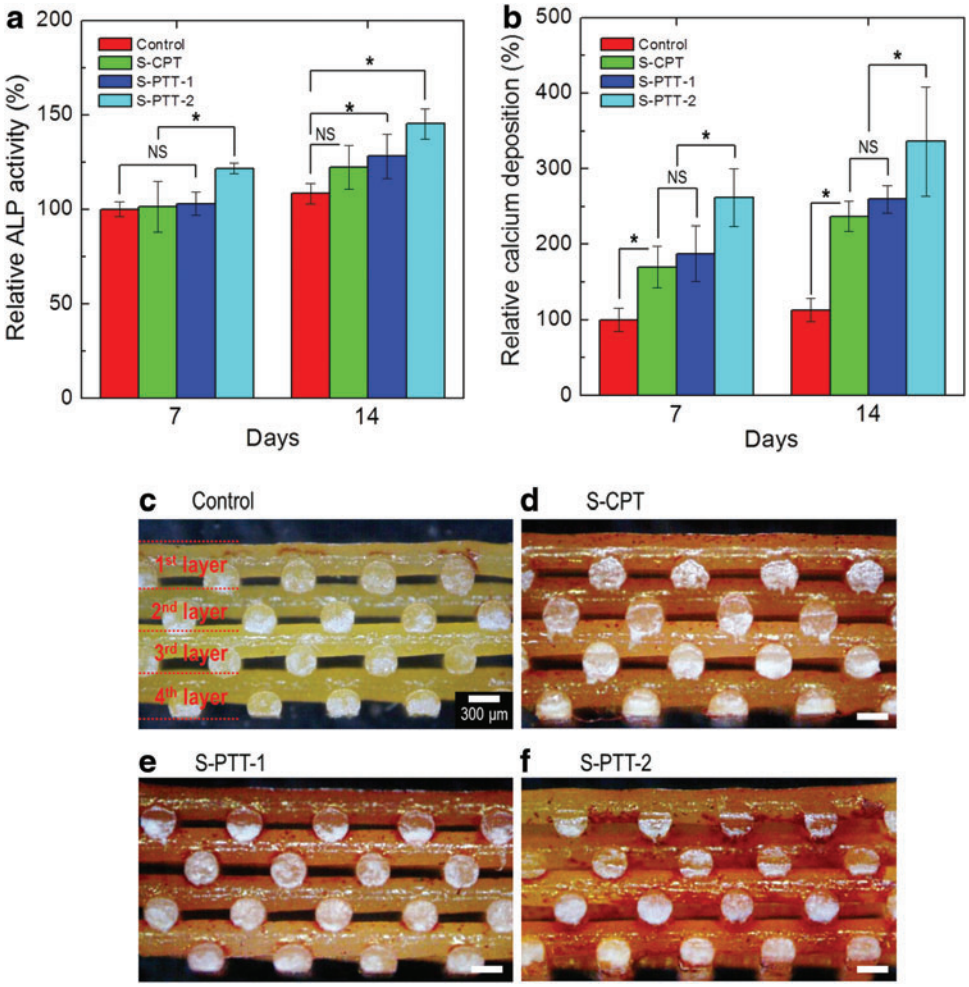

FIG. 9. **(a)** Relative alkaline phosphatase (ALP) activities of MG63 cells on the various scaffolds from 7 to 14 days, and **(b)** relative levels of calcium deposition in the scaffolds. Cross-sectional optical images of ARS staining of **(c)** control, **(d)** S-CPT, **(e)** S-PTT-1, and **(f)** S-PTT-2 scaffolds after 14 days of cell culture. $^*p < 0.05$. Color images available online at www.liebertpub.com/tec

showed a twofold increase in ALP activity.[31] In addition, according to Hatano *et al.*, the optimum roughness (R_a) for osteoblast-like cloned mouse cells (MC3T3-E1) was observed as 810 nm. The roughness value would lead to earlier osteointegration for bone implants.[32] Similarly, the roughness (R_a) of S-PTT-2 was $\sim 654 \pm 71$ nm. Therefore, the roughness of the S-PTT-2 scaffold would be appropriate for osteoblast-like-cells (MG63). However, we could not confirm that this roughness value would be appropriate for all cell types, as the optimum roughness to enhance cellular responses varies depending on several parameters (cell type, surface hardness, etc). The relative ALP activity was compared to the calcium deposition in the scaffolds. Calcium mineralization is evaluated using alizarin red dye. The relative calcium deposition was normalized to the total protein content on scaffolds after 7 and 14 days (Fig. 9b). On days 7 and 14, calcium deposition showed similar trends to ALP activities, but was greater in the plasma-treated PCL mats (S-PTT-1 and S-PTT-2) compared with the control and S-CPT. Similarly, S-PTT-2 showed the highest calcium deposition. As discussed previously, this was likely due to the homogeneously patterned nanosized pits and appropriate roughness value, which may provide favorable microenvironmental conditions for ALP activity and calcium deposition compared with the control and S-CPT.

To qualitatively analyze the influence of calcium deposition, we obtained alizarin red S stained cross-sectional optical images on day 14 of cell culture (Fig. 9c–f). As shown in the optical results, a denser color of alizarin red S staining indicates a higher calcium concentration. The cells on the plasma-treated PCL scaffolds (S-PTT-1 and S-PTT-2) showed greater mineralized matrix deposition compared with the control and S-CPT scaffolds.

To see the influence of cell-culture medium on the ALP activity and precipitation of calcium, the test for the scaffolds in which those were incubated in the same cell-culture

Table 3. Total Protein Contents (Optical Density) of the Scaffolds

	Control	*S-CPT*	*S-PTT-1*	*S-PTT-2*
7 days	0.082 ± 0.005	0.109 ± 0.005	0.121 ± 0.025	0.123 ± 0.024
14 days	0.133 ± 0.011	0.145 ± 0.021	0.154 ± 0.026	0.168 ± 0.022

medium without the cells during 7 and 14 days was conducted. The ALP activity for the control and plasma-treated scaffolds was 2.2–2.8% for 7 and 14 days compared to the ALP activity obtained using the cultured cells in the scaffold for the same periods. In addition, the calcium in the scaffolds from the cell-culture medium was 3.1–3.4% compared to that of cell scaffolds and the value was roughly similar for 7 and 14 days.

Conclusion

Plasma-treated PCL scaffolds fabricated using a novel oxygen plasma treatment method exhibited enhancement of cellular activities, mediated by modulating the hydrophilicity and the nanosized-roughened surface of the scaffolds. By simple modification using a plasma process, the nanosized roughness of the surface of the PCL scaffolds was controllable; this resulted in enhancement of initial cell attachment, proliferation, and differentiation of the MG63 cells. Especially, controlling the surface roughness enhanced the initial cell attachment. This enhanced initial cellular activity accelerated cell proliferation throughout the scaffold, and subsequently increased ALP activity and mineralization. These synergistic effects of hydrophilicity and an appropriately roughened surface enabled creation of newly designed melt-plotted PCL scaffolds. This novel method will facilitate production of polymeric biomaterials that can be applied to hard tissue regeneration. Future work will be directed for the biomineralization in simulated body fluid of the scaffolds treated with the plasma process and evaluation of the performance of the scaffold when used *in vivo*.

Acknowledgments

This study was supported by a grant from the Korea Healthcare Technology R&D Project, Ministry for Health, Welfare, and Family Affairs, Republic of Korea (Grant no. A120942) and also was supported by the National Research Foundation of Korea grant funded by the Ministry of Education, Science, and Technology (MEST) (no. 2012R1A2A2A01017435).

Disclosure Statement

No competing financial interests exist.

References

1. Xu, T., Binder, K.W., Albanna, M.Z., Dice, D., Zhao, W., Yoo, J.J., and Atala, A. Hybrid printing of mechanically and biologically improved constructs for cartilage tissue engineering applications. Biofabrication **5,** 015001, 2013.
2. Yeong, W.Y., Sudarmadji, N., Yu, H.Y., Chua, C.K., Leong, K.F., Venkatraman, S.S., Boey, Y.C. F., and Tan, L.P. Porous polycaprolactone scaffold for cardiac tissue engineering fabricated by selective laser sintering. Acta Biomater **6,** 2028, 2010.
3. Lee, H.J., Ahn, S.H., Bonassar, L.J., Chun, W., and Kim, G.H. Cell-laden poly(ε-caprolactone)/alginate hybrid scaffolds fabricated by an aerosol cross-linking process for obtaining homogeneous cell distribution: fabrication, seeding efficiency, and cell proliferation and distribution. Tissue Eng Part C **19,** 784, 2013.
4. Kim, Y.B., and Kim, G.H. Collagen/alginate scaffolds comprising core (PCL)–shell (collagen/alginate) struts for hard tissue regeneration: fabrication, characterisation, and cellular activities. J Mater Chem B **1,** 3185, 2013.
5. Puppi, D., Chiellini, F., Piras, A.M., and Chiellini, E. Polymeric materials for bone and cartilage repair. Prog Polym Sci **35,** 403, 2010.
6. Zhang, Z.-Y., Teoh, S.H., Teo, E.Y., Chong, M.S.K., Shin, C.W., Tien, F.T., Choolani, M.A., and Chan, J.K.Y. A comparison of bioreactors for culture of fetal mesenchymal stem cells for bone tissue engineering. Biomaterials **31,** 8684, 2010.
7. Abrahamsson, C.K., Yang, F., Park, H., Brunger, J.M., Valonen, P.K., Langer, R., Welter, J.F., Caplan, A.I., Guilak, F., and Freed, L.E. Chondrogenesis and mineralization during *in vitro* culture of human mesenchymal stem cells on three-dimensional woven scaffolds. Tissue Eng Part A **16,** 3709, 2010.
8. Arafat, M.T., Lam, C.X.F., Ekaputra, A.K., Wong, S.Y., Li, X., and Gibson, I. Biomimetic composite coating on rapid prototyped scaffolds for bone tissue engineering. Acta Biomater **7,** 809, 2011.
9. Jacobs, T., Declercq, H., De Geyter, N., Cornelissen, R., Dubruel, P., Leys, C., and Morent, R. Improved cell adhesion to flat and porous plasma-treated poly-ε-caprolactone samples. Surf Coat Technol **232,** 447, 2013.
10. Yildirim, E.D., Pappas, D., Guceri, S., and Sun, W. Accelerated differentiation of osteoblast cells on polycaprolactone scaffolds driven by a combined effect of protein coating and plasma modification. Plasma Process Polym **8,** 256, 2011.
11. Cipitria, A., Skelton, A., Dargaville, T.R., Dalton, P.D., and Hutmacher, D.W. Design, fabrication and characterization of PCL electrospun scaffolds—a review. J Mater Chem **21,** 9419, 2011.
12. Yang, J.Y., Ting, Y.C., Lai, J.Y., Liu, H.L., Fang, H.W., and Tsai, W.B. Quantitative analysis of osteoblast-like cells (MG63) morphology on nanogrooved substrata with various groove and ridge dimensions. J Biomed Mater Res Part A **90,** 629, 2009.
13. Dalby, M.J., Gadegaard, N., Tare, R., Andar, A., Riehle, M.O., Herzyk, P., Wilkinson, C., and Oreffo, R.O.C. The control of human mesenchymal cell differentiation using nanoscale symmetry and disorder. Nat Mater **6,** 997, 2007.
14. Flemming, R.G., Murphy, C.J., Abrams, G.A., Goodman, S.L., and Nealey, P.F. Effects of synthetic micro- and nano-structured surfaces on cell behavior. Biomaterials **20,** 573, 1999.
15. Yim, E.K.F., Reano, R.M., Pang, S.W., Yee, A.F., Chen, C.S., and Leong, K.W. Nanopattern-induced changes in morphology and motility of smooth muscle cells. Biomaterials **26,** 5405, 2005.
16. Sutherland, D.S., Broberg, M., Nygren, H., and Kasemo, B. Influence of nanoscale surface topography and chemistry on the functional behaviour of an adsorbed model macromolecule. Macromol Biosci **1,** 270, 2001.
17. Kumar, G., Waters, M.S., Farooque, T.M., Young, M.F., and Simon, Jr., C.G. Freeform fabricated scaffolds with roughened struts that enhance both stem cell proliferation and differentiation by controlling cell shape. Biomaterials **33,** 4022, 2012.
18. Domingos, M., Intranuovo, F., Gloria, A., Gristina, R., Ambrosio, L., Bartolo, P.J., and Favia, P. Improved

osteoblast cell affinity on plasma-modified 3-D extruded PCL scaffolds. Acta Biomater **9,** 5997, 2013.
19. Yeo, M.G., Simon, Jr., C.G., and Kim, G.H. Effects of offset values of solid freeform fabricated PCL–β-TCP scaffolds on mechanical properties and cellular activities in bone tissue regeneration. J Mater Chem **22,** 21636, 2012.
20. Sobral, J.M., Caridade, S.G., Sousa, R.A., Mano, J.F., and Reis, R.L. Three-dimensional plotted scaffolds with controlled pore size gradients: Effect of scaffold geometry on mechanical performance and cell seeding efficiency. Acta Biomater **7,** 1009, 2011.
21. Murphy, C.M., Haugh, M.G., and O'Brien, F.J. The effect of mean pore size on cell attachment, proliferation and migration in collagen–glycosaminoglycan scaffolds for bone tissue engineering. Biomaterials **31,** 461, 2010.
22. Lord, M.S., Foss, M., and Besenbacher, F. Influence of nanoscale surface topography on protein adsorption and cellular response. Nano Today **5,** 66, 2010.
23. Han, M., Sethuraman, A., Kane, R.S., and Belfort, G. Nanometer-scale roughness having little effect on the amount or structure of adsorbed protein. Langmuir **19,** 9868, 2003.
24. Dalby, M.J., Andar, A., Nag, A., Affrossman, S., Tare, R., McFarland, S., and Oreffo, R.O.C. Influence of nanoscale surface topography on protein adsorption and cellular response. J R Soc Interface **5,**1055, 2008.
25. Nandakumar, A., Birgani, Z.T., Santos, D., Mentink, A., Auffermann, N., van der Werf, K., Bennink, M., Moroni, L., van Blitterswijk, C., and Habibovic, P. Surface modification of electrospun fibre meshes by oxygen plasma for bone regeneration. Biofabrication **5,** 015006, 2013.
26. Hollister, S.J. Porous scaffold design for tissue engineering. Nat Mater **4,** 518, 2005.
27. Srinivasan, S., Jayasree, R., Chennazhi, K.P., Nair, S.V., and Jayakumar, R. Biocompatible alginate/nano bioactive glass ceramic composite scaffolds for periodontal tissue regeneration. Carbohydr Polym **87,** 274, 2012.
28. Gibson, L.J., and Ashby, M.F. The mechanics of foams: basic results. In: Cellular Solids. Oxford, UK: Cambridge University Press, 1997, p. 175.
29. Declercq, H.A., Desmet, T., Berneel, E.E.M., Dubruel, P., and Cornelissen, M.J. Synergistic effect of surface modification and scaffold design of bioplotted 3-D poly-ε-caprolactone scaffolds in osteogenic tissue engineering. Acta Biomater **9,** 7699, 2013.
30. Thevenot, P., Nair, A., Dey, J., Yang, J., and Tang, L. Method to analyze three-dimensional cell distribution and infiltration in degradable scaffolds. Tissue Eng Part C **14,** 319, 2008.
31. Jeon, H.J., and Kim, G.H. Effects of a cell-imprinted poly(dimethylsiloxane) surface on the cellular activities of MG63 osteoblast-like cells: preparation of a patterned surface, surface characterization, and bone mineralization. Langmuir **28,** 13423, 2012.
32. Hatano, K., Inoue, H., Kojo, T., Matusunaga, T., Tsujisawa, T., Uchiyama, C., and Uchida, Y. Effect of surface roughness on proliferation and alkaline phosphatase expression of rat calvarial cells cultured on polystyrene. Bone **25,** 439, 1999.

Address correspondence to:
GeunHyung Kim, PhD
Department of Bio-Mechatronic Engineering
College of Biotechnology and Bioengineering
Sungkyunkwan University
Suwon 440-746
South Korea

E-mail: gkimbme@skku.edu

Received: November 14, 2013
Accepted: March 10, 2014
Online Publication Date: April 21, 2014